Two-Photon Photovoltaic Effect in Silicon

Sasan Fathpour, *Member, IEEE*, Kevin K. Tsia, *Member, IEEE*, and Bahram Jalali, *Fellow, IEEE*

***Abstract*—Optical amplification, wavelength conversion, and a myriad of other functions that were once considered to be beyond silicon's reach have been made possible by the material's nonlinear optical properties. The common feature of such devices is the high optical intensity that is required to induce the nonlinear optical interactions. Concurrent with the useful nonlinearities (Raman and Kerr) are two-photon absorption and free carrier scattering, which are two related and harmful phenomena that render silicon lossy at high intensities. This paper explores the use of the two-photon photovoltaic effect as a means to counter these phenomena in an energy-efficient manner. The effect reduces losses due to free carrier scattering and serendipitously scavenges the optical energy lost to two-photon absorption. Analytical and numerical modeling of the two-photon photovoltaic effect in silicon devices is presented. The model is validated through comparison with experimental results and is used to establish the limits of this approach for creating energy-efficient silicon photonic devices.**

***Index Terms*—Energy harvesting, Kerr effect, nonlinear optics, optical amplifiers, photovoltaic effect, Raman effect, silicon photonics, two-photon absorption.**

I. Introduction

SILICON photonics has been the topic of immense interest, a trend that is fueled by the desire to create low-cost photonic devices by tapping into the vast silicon manufacturing infrastructure. The recent developments have been documented in numerous reviews, two recent examples of which are [1] and [2].

Some of the most dramatic progress has been made by recognizing and exploiting nonlinear optical properties of silicon. This has led to demonstrations of optical amplification and lasing [3]–[6], continuum generation [7]–[9], and wavelength conversion and parametric amplification [10]–[14], all within the past five years. Such functions were once perceived to be beyond the capabilities of silicon, and they add to a powerful device toolbox that also includes optical filters, electrooptic modulators, and photodetectors.

Despite the plethora of new devices that have been proposed and investigated, virtually no attention has been paid to their power dissipation and its implications. This is particularly relevant in the context of the aforementioned nonlinear optical devices, where high pump intensities are required to induce the requisite Kerr and Raman nonlinearities. In such devices, high intensities impose a twofold energy-efficiency crisis. First, optical power is converted to heat through the two-photon absorption (TPA) process. Second, free carriers generated by TPA must be actively removed from the waveguide core region, otherwise they will accumulate, cause severe free carrier absorption (FCA), and will prevent continuous-wave (CW) operation [15], [16]. Carrier sweep-out is typically achieved using a reverse-biased p-n junction [6]. This results in electrical power dissipation and adds to the optical power dissipation caused by the TPA. Reducing the carrier lifetime, by introducing crystal defects, can alleviate the carrier accumulation [17], [18]. However, eliminating the need for carrier sweep-out requires a lifetime that is of the order of 100 ps [19]. Presently, it is not clear whether such low lifetimes can be achieved without a pronounced increase in optical losses [18].

This paper addresses the power dissipation resulting from the deleterious TPA and the active carrier sweep-out in silicon photonic devices and examines the prospects of two-photon photovoltaic (TPP) effect as a potential solution. The paper describes, for the first time, analytical and numerical modeling of this phenomenon in silicon Raman amplifiers leading to quantitative assessment of its efficacy. To validate the model, its predictions are compared with our experimental results, some of which have appeared in previous publications [20], [21]. The model is also employed as a tool to study the theoretical limits of the TPP effect.

II. Model

Energy harvesting in nonlinear silicon photonic devices is achieved by collecting the TPA-generated carriers by means of a p–n junction diode that is biased in the fourth quadrant (current $I < 0$ and voltage $V > 0$) of its current–voltage (I–V) characteristics (Fig. 1). Conceptually, the TPP effect is a nonlinear equivalent of the conventional photovoltaic effect of solar cells but with certain differences. High optical intensities are required for the onset of the nonlinear effect, and two photons are involved for generating one electron–hole pair, thus the collection efficiency cannot exceed 50%. Also, structural and geometrical differences with conventional photovoltaic devices demand alterations in the theoretical model that is typically used to describe solar cells.

As shown in Fig. 1(a), TPP effect devices are based on waveguides with lateral p–n junction diodes, in which the pump power is nonlinearly lost due to TPA and FCA along the z-direction perpendicular to the junction x–y cross section. Thus, unlike a solar cell which can be conveniently modeled as a one-dimensional (1-D) device [22], the present problem requires a minimum of a 2-D approach. The nonlinear propagation of the coupled optical intensity $I_p(z)$ is governed by [16]

$$\frac{dI_p(z)}{dz} = -(\alpha + \alpha_{\mathrm{FCA}}(z))I_p(z) - \beta {I_p}^2(z) \qquad (1)$$

where β is the TPA coefficient and α is the linear absorption coefficient of the waveguide. The wavelength λ and dependency

Manuscript received March 24, 2007; revised July 18, 2007. This work was supported by the Defense Advanced Research Projects Agency.

The authors are with the Electrical Engineering Department, University of California, Los Angeles, CA 90095-1594 USA (e-mail: sasan@eelucla.edu).

Digital Object Identifier 10.1109/JQE.2007.907545

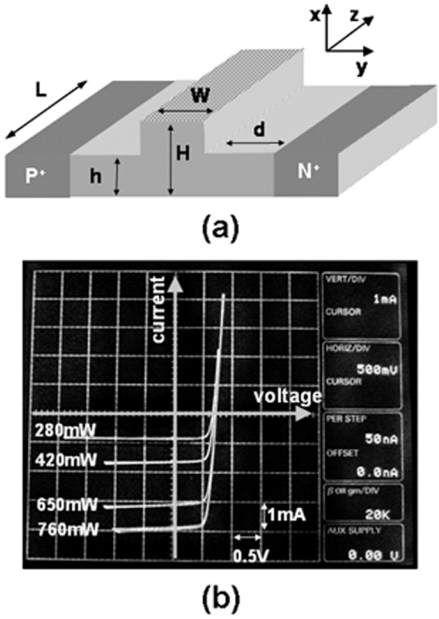

Fig. 1. (a) Schematic of a silicon waveguide with a p–n junction diode. The values of the shown geometrical dimensions are given in Table I. (b) Current–voltage characteristics of the fabricated p–n diodes measured with a curve tracer at various coupled pump powers, showing photovoltaic effect in the fourth quadrant (current < 0 and voltage > 0).

TABLE I
DEVICE DIMENSIONS AND PARAMETERS AND MATERIAL PROPERTIES

Parameter	Value	Unit
L	2.2	cm
W	1.5	μm
H	2.0	μm
d	1.9	μm
h	1.1	μm
N^+, P^+	1x10^{19}	cm^{-3}
E_p	0.8	eV
β	0.7	cm/GW
g_R	15	cm/GW
μ_n	1332	cm^2/V-s
μ_p	455	cm^2/V-s
τ_n, τ_p	15	ns
α	0.5	dB/cm
$\eta_{coupling}$	0.42	–

of the FCA coefficient $\alpha_{\rm FCA}$ (in cm^{-1}) is given by Soref's expression [23]

$$\alpha_{\rm FCA} = \Delta\alpha_e + \Delta\alpha_h = (8.5 \times 10^{-18} \cdot \Delta N + 6.0 \times 10^{-18} \cdot \Delta P) \cdot (\lambda/1.55)^2 \quad (2)$$

where ΔN and ΔP are the free electron and hole concentrations (in cm^{-3}), respectively, and are functions of $I_p(z)$ and bias voltage V.

The carrier photogeneration rate from TPA in the waveguide core is $G = dN/dt = -(1/2E_p)dI_p/dz = \beta I_p^2/2E_p$, where E_p is the photon energy. The corresponding photocurrent per unit length is $qA_{\rm eff}G$, where $A_{\rm eff}$ is the effective area of the waveguide and q is the electron charge. The total photocurrent in a waveguide with length L is expressed as

$$I_G = \frac{-q\beta A_{\rm eff}}{2E_p}\int_o^L I_p^2(z)dz \equiv \frac{-q\beta A_{\rm eff}}{2E_p} L_{\rm NL} I_{p0}^2 \quad (3)$$

where I_{p0} denotes the coupled pump intensity at $z = 0$. The nonlinear photovoltaic effect is implicit in this last expression, as it is quantified in terms of the defined effective length

$$L_{\rm NL} \equiv \int_0^L \frac{I_p^2(z)}{I_{p0}^2} dz. \quad (4)$$

This important quantity is the nonlinear equivalent of the interaction length commonly defined in optical fibers [24].

If the photodiode is biased in the fourth quadrant of its I–V characteristics [Fig. 1(b)], I_G can be collected with negative power dissipation, i.e., the energy of the pump lost to TPA can be harvested. In order to analyze the power generation and efficiency of this photovoltaic process, the contributions of carrier injection and recombination to the total current need to be considered. The minority carrier diffusion terms can be conveniently calculated from the celebrated Shockley equation

$$I_D = qhL \times \left(\frac{D_n n_{p0}}{L_n} + \frac{D_p p_{n0}}{L_p}\right)(e^{qV/kT} - 1) \quad (5)$$

where h and L dimensions are depicted in Fig. 1(a) and the other parameters have the usual meanings [25]. The Shockley equation is valid, since photogeneration in the N$^+$ and P$^+$ doped regions is negligible in the p–n diode. This contrasts the conventional solar cell theory, where photogeneration predominantly occurs in the N and P doped regions, and a more detailed solution of the minority carrier diffusion equations is required [22].

Another implication of the p-i-n structure is that the recombination model in the intrinsic region of the present device resembles the one used for a forward-biased thyristor (on state) [25]. In this approximation of the Shockley–Read–Hall recombination, the rate is given by $R = \Delta N/\tau_R$, which is valid for $\Delta N = \Delta P >> n_i$. Ignoring the Auger coefficient, τ_R equals the ambipolar lifetime $\tau_n + \tau_p$, where τ_n and τ_p are electron and hole bulk recombination lifetimes, respectively [25]. Consequently, the recombination current is given by

$$I_R = \frac{qh(W+2d)}{\tau_n+\tau_p}\int_0^L \overline{\Delta N}(z)dz \equiv \frac{qh(W+2d)LN_{\rm eff}}{\tau_n+\tau_p} \quad (6)$$

where $W + 2d$ is the width of the intrinsic region in Fig. 1(a). The defined $N_{\rm eff}$ is an effective carrier density along z, similar to the discussed $L_{\rm NL}$. It is implied in (6) that $\overline{\Delta N}(z)$ is an average value in the x–y plane.

Surface recombination at the Si/SiO$_2$ interfaces is an important effect in SOI micrometer and submicrometer waveguides

and can indeed be a more dominant factor than bulk recombination in the effective lifetime τ_{eff} [26]. A more elaborate analysis of the TPP effect should thus consider the contribution of surface recombination to the total current. However, the values of surface recombination velocities are not easily measurable and vary considerably according to the employed fabrication technique and conditions [27], [28]. Alternatively, the value of τ_{eff} can be estimated from waveguide loss measurements as well as from pump-probe experiments [29]. We have measured the lifetime in our fabricated waveguides using the latter technique, yielding a value of 15 ns. In the theoretical analysis of (5) and (6), we assume that all of the bulk and surface recombination processes are lumped into this measured value, i.e., $\tau_n = \tau_p = \tau_{\text{eff}} = 15$ ns. It is noteworthy that the effective lifetime value is smaller ($\sim$1 ns) in submicrometer waveguides [30]. As mentioned before, introducing lattice defects through implantation can decrease τ_{eff} as well [17], [18]. Effective lifetime values as low as 150 ps have been reported in submicrometer waveguides enhanced with argon implantation [18].

The total photodiode current is expressed as $I_T = I_G + I_D + I_R$. The dissipated power is given by $P = V \times I_T(V)$. The bias V_m at which power generation is maximized in the fourth quadrant of power–voltage (P–V) characteristics is determined from $\partial P/\partial V = 0$. If $I_D, I_R << I_G$ at $V \approx V_m$, then

$$P_m \approx -V_m \times I_G(V_m) = \frac{q\beta A_{\text{eff}}}{2E_p} V_m L_{\text{NL}} I_{p0}^2. \tag{7}$$

The collection efficiency η_c is the number of collected carriers per number of photons consumed by TPA as

$$\begin{aligned}\eta_c =& \frac{I_T}{2I_G} \\ =& \frac{1}{2} - hLE_p \\ & \times \frac{\left(\frac{D_n n_{p0}}{L_n} + \frac{D_p p_{n0}}{L_p}\right)(e^{qV/kT} - 1) + \frac{(W+2d)N_{\text{eff}}}{\tau_n + \tau_p}}{\beta A_{\text{eff}} L_{\text{NL}} I_{p0}^2}.\end{aligned} \tag{8}$$

The factor of 2 in $I_T/2I_G$ accounts for the fact that two absorbed photons create one electron–hole pair. The TPA coefficient β is readily recognized as the key material parameter that determines the maximum generated power and the corresponding efficiency. Also, the defined nonlinear length is recognized as an important figure of merit in the performance of the TPP effect. The dependence of P_m and η_c on absorptions due to linear loss and free-carrier scattering is implicit in L_{NL}. In other words, higher α and/or α_{FCA} lead to smaller L_{NL}.

In Section III, the quantitative predictions of the above theory are presented and compared with experimental results. A fully analytical analysis is, however, difficult to perceive because of the nonlinear nature of the problem apparent in the L_{NL} and N_{eff} quantities. Hence, these two values are evaluated using a commercial drift-diffusion simulator (ATLAS by Silvaco International), as follows. TPA was emulated by specifying a carrier generation rate at the waveguide core. The simulator provides the carrier concentrations as a function of V and I_p, which are averaged in the x–y plane of the waveguide core being used in (2) and (6). In order to accommodate for the nonlinear nature of the problem, a quasi-3-D model was developed in which the 2-D results of ATLAS at several optical intensities were interpolated to numerically solve (1), and finally evaluate L_{NL} and N_{eff}.

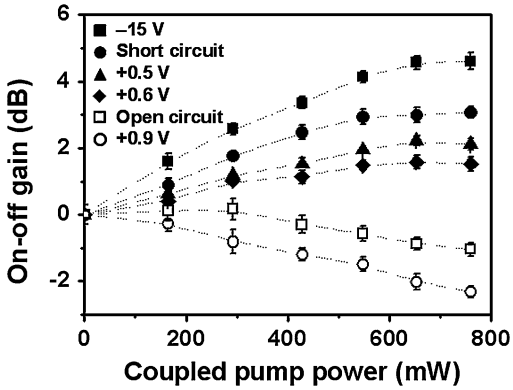

Fig. 2. Measured on–off Raman gain versus coupled pump power in the devices of Fig. 1 at different biasing conditions.

A fully simulation-based analysis is also performed for comparison. The diode current per unit length $J(A/\mu m)$ is provided by ATLAS, from which the total current can be calculated from $I_T = \int_0^L J(I_p(z))dz$. It is assumed in this last expression that the ohmic loss of the contacts are negligible and that the current vector has no z-component. The latter is a fair approximation at sufficiently low biases at which there is no voltage drop along the waveguide.

III. Results and Discussion

We have demonstrated energy harvesting in silicon Raman amplifiers and in wavelength converters based on the Kerr effect [20], [21], [31]. The details of device fabrication and experiments can be found elsewhere [20], but are briefly reviewed here for completeness. The dimensions of the fabricated devices depicted in Fig. 1(a) are reported in Table I. Linear loss of $\alpha \sim 0.5$ dB/cm was measured in the waveguide using the Fabry–Perot technique.

Fig. 2 presents the measured on–off Raman gain at different coupled pump powers and biasing conditions. The pump is an external-cavity tunable diode laser at 1539 nm with a linewidth of 0.1–0.2 nm amplified with an erbium-doped fiber amplifier (EDFA). The Stokes signal is a 1673-nm distributed feedback (DFB) laser biased at an output power of $\sim$4.5 mW. A maximum on–off gain of $\sim$4.5 dB is obtained at a reverse bias of 15 V. A Raman gain of $\sim$3 dB is attained when the diode is short-circuit (0 V), i.e., zero power dissipation [32]. More importantly, on–off Raman gains of more than 2 dB is measured, when the device is forward-biased at voltages ≤ 0.7 V. The importance of this biasing regime is that power dissipation is negative. For instance, $\sim$2 mW of electrical power is generated at a bias of $+0.5$ V. In contrast, $\sim$150 mW is dissipated at -15 V. Clearly, the TPP effect offers an energy-efficient solution for nonlinear silicon photonics.

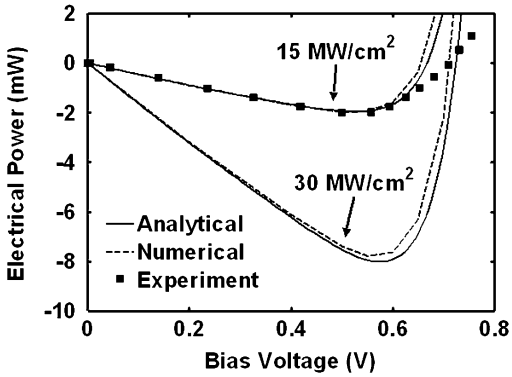

Fig. 3. Power–voltage characteristics of the diodes at two coupled pump intensities for analytical expressions (solid line), numerical simulations (dashed line), and experiment (squares).

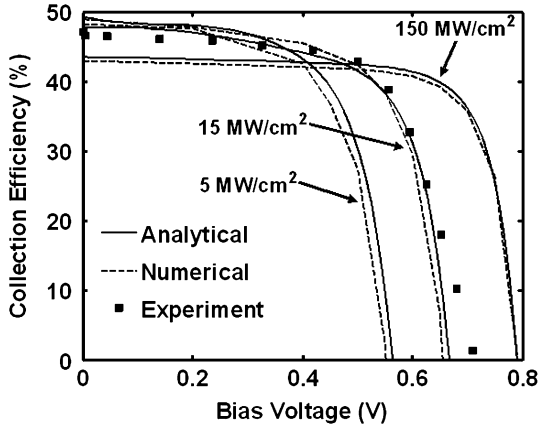

Fig. 4. Collection efficiency of the photovoltaic effect at three pump intensities for analytical expressions (solid line), numerical simulations (dashed line), and experiment (squares).

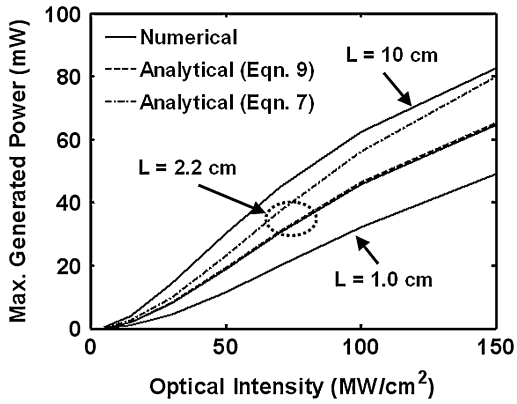

Fig. 5. Simulated maximum power generation (solid lines) versus coupled pump intensity for three different device lengths of 1.0, 2.2, and 10 cm. Also shown are the analytical values from the approximate form in (7) (dot-dashed line) and the exact expression in (9) (dashed line) for the 2.2-cm case.

The TPA-induced photovoltaic effect is clearly evidenced in the fourth quadrant of the I–V characteristics in Fig. 1(b), measured by a curve tracer. The attenuated pump intensity via TPA creates free carriers in the SOI waveguide. The collected photogenerated carriers contribute to a current component that delivers electrical power to the external circuitry. Therefore, the sweep-out of TPA-generated free carriers by the built-in field of the junction can be exploited to generate electrical power. Similar energy harvesting was demonstrated in wavelength converters, based on the Kerr effect, on the same devices [31]. We have also proposed an electrooptical modulator that achieves negative static power dissipation by exploiting the TPP effect [33].

The results obtained from the model developed in Section II for the TPP effect are presented herein and compared with experiments. Fig. 3 shows the theoretical P–V characteristics of the diodes in Fig. 1(a) with identical dimensions to our experiments (Table I). The material parameters used in the analysis are also summarized in the same table. The agreement between the fully simulated results and the analytical model described in Section II is clear, thanks to the effective nonlinear quantities $L_{\rm NL}$ and $N_{\rm eff}$ borrowed for the analytical model from the simulations. The experimental P–V results—extracted from the measured current and voltage drop across the diode—are also presented for $I_{p0} = 15$ MW/cm^2. The theoretical results show excellent agreement with experiment at biases in the fourth quadrant of the P–V characteristics, which is the regime of interest in this study. The deviation between experiment and theory in the first quadrant is possibly due to the contact ohmic loss at high forward biases, which is ignored in the theoretical analysis.

Collection efficiency η_c is plotted versus voltage at different pump intensities in Fig. 4. Again, good agreement between the analytical model, the numerical simulation, and the experimental results is observed. The experimental value of η_c was extracted from the measured photocurrent and the estimated pump power inside the waveguide, obtained from waveguide loss measurements. As $V \rightarrow 0$ at lower pump intensities, η_c approaches the theoretical limit of 50% predicted by (8). This is not the case for the high pump intensity of 150 MW/cm^2, at which $\eta_c \approx 43\%$ for $V \approx 0$. This decrease of η_c at $V \approx 0$ and high pump intensities is attributed to the decrease of nonlinear length $L_{\rm NL}$, as will be discussed further below. The value of η_c at maximum power generation bias V_m is extracted to be within 39%–41% and is nearly independent of coupled optical intensity from 5 to 150 MW/cm^2. Physically, this rather constant behavior is because the recombination current dominates the diffusive current at low biases and grows at approximately the same rate as the photogenerated current, i.e., $I_D << I_R, I_G$ and $N_{\rm eff} \propto L_{\rm NL} I_{p0}^2$ at $V \leq V_m$ in (8).

Fig. 5 presents the simulated maximum generated power versus coupled pump intensity for three different device lengths. The exact analytical values obtained from

$$P_m = -V_m \times I_T(V_m) \tag{9}$$

and the approximation form in (7) are also shown (only for $L = 2.2$ cm case). The P_m values predicted by (7) deviate from the exact analytical and numerical values at higher intensities but nonetheless offer a convenient first-order estimate of the harvested power. A quadratic dependence of P_m on pump intensity may be expected from (7), which is not the case. The

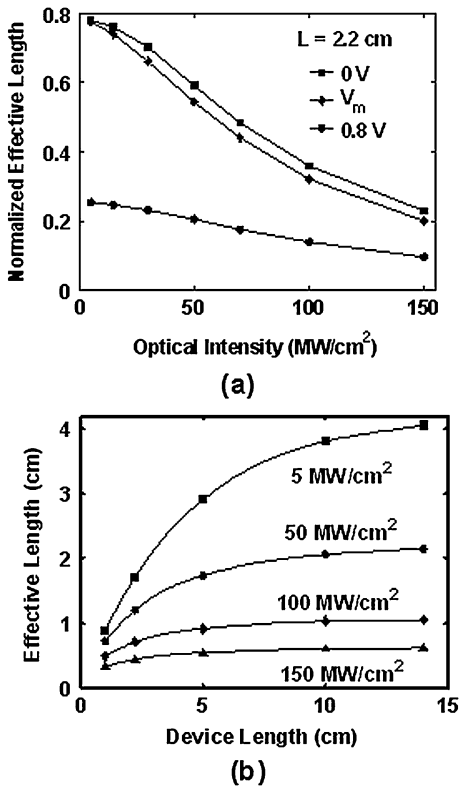

Fig. 6. (a) Normalized effective length $L_{\rm NL}/L$ versus coupled pump intensity at short circuit or 0 V (squares), maximum power generation bias or V_m (diamonds), and a first-quadrant forward bias of 0.8 V (circles). The waveguide length is $L = 2.2$ cm and V_m varies from 0.43 to 0.62 V for the shown optical intensity range. (b) Effective length $L_{\rm NL}$ versus device length L at different optical intensities and at maximum power generation bias V_m. Solid lines are fittings to the simulated data.

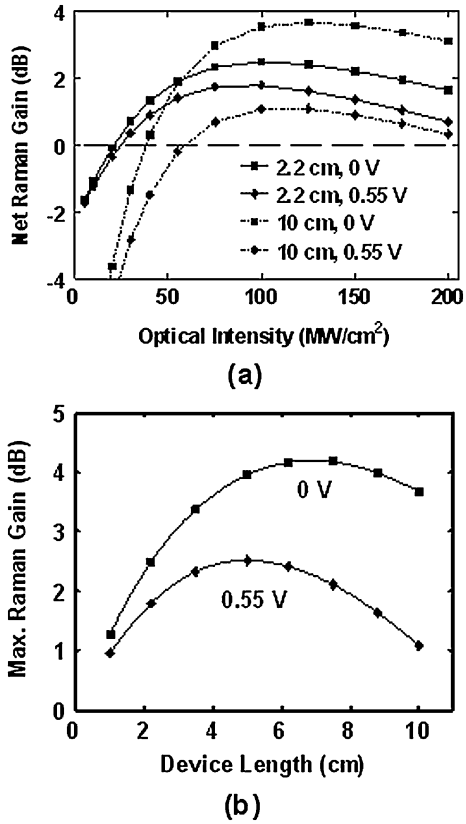

Fig. 7. (a) Simulated net Raman gain versus coupled pump intensity at short-circuit or 0 V (squares), and 0.55 V (diamonds) for devices with lengths of 2.2 cm (solid line) and 10 cm (dot-dashed line). (b) Maximum attainable net Raman gain versus device length for the same biases. Solid lines are fittings to the simulated data.

nonlinear decrease of $L_{\rm NL}$ with pump intensity is responsible for the rather linear dependence of P_m, as follows.

Fig. 6(a) plots the dependence of the normalized effective length $L_{\rm NL}/L$ on the pump intensity at 0 V, V_m and 0.8 V for $L = 2.2$ cm. It is seen that, at $V \leq V_m$, the normalized length is 0.55–0.8 for intensities ≤ 50 MW/cm^2, but decreases to as low as 0.2 at 150 MW/cm^2. At a typical deep forward (first quadrant) bias of 0.8 V, current injection is so high that $L_{\rm NL} < 0.25L$, even at very low pump intensities. This finding may be of interest in the design of variable optical attenuators and those silicon optical modulators that operate based on carrier injection in forward bias [33], [34]. Moreover, a longer device does not necessarily increase the performance of the TPP effect. Fig. 6(b) plots the effective length versus device length at different coupled pump intensities, showing a strong saturation trend, especially at high intensities. Strong saturation was also observed in the attainable harvested electrical power for $L > 10$ (which is not shown in Fig. 5). Physically, $L \sim 10$ cm is long enough for the absorption of virtually all of the pump energy for $I_{p0} > \sim 50$ MW/cm^2.

The theoretical model of the TPP effect presented here is applicable to a wide range of nonlinear devices including those based on Raman and Kerr effects. Under small-signal conditions, (1) is still a valid approximation for the propagation of the pump beam, as pump depletion due to energy transfer to Stokes is small [16]. The evolution of Stokes intensity I_s is given by [16]

$$\frac{dI_s(z)}{dz} = -(\alpha + \alpha_{\rm FCA}(z))I_s(z) + (g_R - 2\beta)I_p(z)I_s(z) \tag{10}$$

where g_R is the Raman gain coefficient (Table I). The wavelength dependence of $\alpha_{\rm FCA}$ for pump (1539 nm) and Stokes (1673 nm) was taken into account to solve (1) and (10) simultaneously. Fig. 7(a) presents the calculated net Raman gain versus coupled pump intensity for $L = 2.2$ cm and 10 cm at two different biases. Gain values of 2.5 and 1.8 are attainable at short-circuit (0 V) and 0.55 V, respectively, for $L = 2.2$ cm, occurring at $I_{p0} \sim$ 90–100 MW/cm^2. The gain decreases at higher pump intensities due to an increase in $\alpha_{\rm FCA}$.

The device lengths of Fig. 7(a) are not the optimum values for maximum Raman gain. Fig. 7(b) presents the maximum attainable gain versus device length, which is obtained from the peaks of plots similar to Fig. 7(a). Optimum lengths of $\sim$6.5 and $\sim$5 cm are recognized for short-circuit and 0.55-V biases, respectively. The corresponding maximum net gain values are 4.2 and 2.5 dB, respectively. Maximum gain occurs at typical intensities of 90 to 125 MW/cm^2, depending on the bias and device length.

IV. Conclusion

In summary, TPA and the resulting free-carrier scattering are omnipresent problems in silicon photonic devices that operate based on nonlinear optical interactions, e.g., Raman and Kerr. The TPP effect can be employed to harvest electrical energy from silicon photonic devices based on these nonlinear effects. A herein defined nonlinear effective length is recognized as an important parameter in the analysis and design of such devices. The electron–hole collection efficiency of the process is recognized to be $\sim$40% and is almost independent of the coupled optical intensity in the 5–150-MW/cm^2 range. Maximum Raman gain is achievable at pump intensities of 90–125 MW/cm^2 for optimum device lengths of 5–7 cm (depending on the bias), which is a limit range beyond which gain decreases due to carrier screening by photogenerated carriers.

References

[1] L. Pavesi and G. Guillot, Eds., *Optical Interconnects: The Silicon Approach*, ser. Springer Series in Optical Sciences. Berlin, Germany: Springer-Verlag, 2006, vol. 119.

[2] B. Jalali and S. Fathpour, "Silicon photonics," *J. Lightw. Technol.*, vol. 24, no. 12, pp. 1400–1415, Dec. 2006.

[3] R. Claps, D. Dimitropoulos, Y. Han, and B. Jalali, "Observation of Raman emission in silicon waveguides at 1.54 μm," *Opt. Exp.*, vol. 10, pp. 1305–1313, Nov. 2002.

[4] R. Claps, D. Dimitropoulos, V. Raghunathan, Y. Han, and B. Jalali, "Observation of stimulated Raman scattering in silicon waveguides," *Opt. Exp.*, vol. 11, pp. 1731–1739, Jul. 2003.

[5] O. Boyraz and B. Jalali, "Demonstration of a silicon Raman laser," *Opt. Exp.*, vol. 12, pp. 5269–5273, Oct. 2004.

[6] H. Rong, R. Jones, A. Liu, O. Cohen, D. Hak, A. Fang, and M. Paniccia, "A continuous-wave Raman silicon laser," *Nature*, vol. 433, pp. 725–728, Feb. 2005.

[7] O. Boyraz, T. Indukuri, and B. Jalali, "Self-phase modulation-induced spectral broadening in silicon waveguides," *Opt. Exp.*, vol. 12, pp. 829–834, Mar. 2004.

[8] I. Hsieh, X. Chen, J. I. Dadap, N. C. Panoiu, R. M. Osgood, S. J. McNab, and Y. A. Vlasov, "Ultrafast-pulse self-phase modulation and third-order dispersion in Si photonic wire-waveguides," *Opt. Exp.*, vol. 14, pp. 12380–12387, Dec. 2006.

[9] L. Yin, Q. Lin, and G. P. Agrawal, "Soliton fission and supercontinuum generation in silicon waveguides," *Opt. Lett.*, vol. 32, pp. 391–393, Jan. 2007.

[10] R. Claps, V. Raghunathan, D. Dimitropoulos, and B. Jalali, "Anti-Stokes Raman conversion in silicon waveguides," *Opt. Exp.*, vol. 11, pp. 2862–2872, Nov. 2003.

[11] R. L. Espinola, J. I. Dadap, R. M. Osgood, Jr., S. J. McNab, and Y. A. Vlasov, "C-band wavelength conversion in silicon photonic wire waveguides," *Opt. Exp.*, vol. 13, pp. 4341–1049, May 2005.

[12] K. Yamada, H. Fukuda, T. Tsuchizawa, T. Watanabe, T. Shoji, and S. Itabashi, "All-optical efficient wavelength conversion using silicon photonic wire waveguide," *IEEE Photon. Technol. Lett.*, vol. 18, no. 5, pp. 1046–1048, May 2006.

[13] H. Rong, Y.-H. Kuo, A. Liu, M. Paniccia, and O. Cohen, "High efficiency wavelength conversion of 10 Gb/s data in silicon waveguides," *Opt. Exp.*, vol. 14, pp. 1182–1188, Feb. 2006.

[14] M. A. Foster, A. C. Turner, J. E. Sharping, B. S. Schmidt, M. Lipson, and A. L. Gaeta, "Broad-band optical parametric gain on a silicon photonic chip," *Nature*, vol. 441, pp. 960–963, Jun. 2006.

[15] T. K. Liang and H. K. Tsang, "Role of free carriers from two-photon absorption in Raman amplification in silicon-on-insulator waveguides," *Appl. Phys. Lett.*, vol. 84, pp. 2745–2747, Feb. 2004.

[16] R. Claps, V. Raghunathan, D. Dimitropoulos, and B. Jalali, "Influence of nonlinear absorption on Raman amplification in Silicon waveguides," *Opt. Exp.*, vol. 12, pp. 2774–2780, Jun. 2004.

[17] Y. Liu and H. K. Tsang, "Raman gain in helium ion implanted silicon waveguides," presented at the IEEE Conf. Lasers and Electro-Optics (CLEO), 2006, Paper CTuU6.

[18] K. Yamada, H. Fukuda, T. Watanabe, T. Tsuchizawa, H. Shinojima, T. Tanabe, M. Takahashi, and S. Itabashi, "All-optical wavelength conversion using silicon photonic wire waveguide," in *Proc. IEEE Group IV Photon. Conf.*, 2006, pp. 237–239.

[19] B. Jalali, "Teaching silicon new tricks," *Nature Photon.*, vol. 1, pp. 193–195, Apr. 2007.

[20] S. Fathpour, K. K. Tsia, and B. Jalali, "Energy harvesting in silicon Raman amplifiers," *Appl. Phys. Lett.*, vol. 89, p. 061109, Aug. 2006.

[21] S. Fathpour, K. K. Tsia, and B. Jalali, "Photovoltaic effect in silicon Raman amplifiers," in *Proc. Optical Amplifiers and Their Applications (OAA 2006)*, 2006, paper# PD1.

[22] J. Nelson, *The Physics of Solar Cells*. London, U.K.: Imperial College, 2003.

[23] R. A. Soref and B. R. Bennett, "Kramers-Kronig analysis of E-O switching in silicon," *Proc. SPIE*, vol. 704, pp. 32–37, 1986.

[24] G. P. Agrawal, *Nonlinear Fiber Optics*, 3rd ed. New York: Academic, 2001.

[25] S. M. Sze, *Physics of Semiconductor Devices*, 2nd ed. New York: Wiley, 1981.

[26] D. Dimitropoulos, R. Jhaveri, R. Claps, J. C. S. Woo, and B. Jalali, "Lifetime of photogenerated carriers in silicon-on-insulator rib waveguides," *Appl. Phys. Lett.*, vol. 86, p. 071115, Feb. 2005.

[27] O. Palais and A. Arcari, "Contactless measurement of bulk lifetime and surface recombination velocity in silicon wafers," *J. Appl. Phys.*, vol. 93, pp. 4686–4690, Apr. 2003.

[28] T. Kuwayama, M. Ichimura, and E. Arai, "Interface recombination velocity of silicon-on-insulator wafers measured by microwave reflectance photoconductivity decay method with electric field," *Appl. Phys. Lett.*, vol. 83, pp. 928–930, Aug. 2003.

[29] R. Claps, V. Raghunathan, O. Boyraz, P. Koonath, D. Dimitropoulos, and B. Jalali, "Raman amplification and lasing in SiGe waveguides," *Opt. Exp.*, vol. 13, pp. 2459–2466, Apr. 2005.

[30] R. Espinola, J. Dadap, R. Osgood, Jr., S. McNab, and Y. Vlasov, "Raman amplification in ultrasmall silicon-on-insulator wire waveguides," *Opt. Exp.*, vol. 12, pp. 3713–3718, Aug. 2004.

[31] K. K. Tsia, S. Fathpour, and B. Jalali, "Energy harvesting in silicon wavelength converter," *Opt. Exp.*, vol. 14, pp. 12327–12333, Dec. 2006.

[32] S. Fathpour, O. Boyraz, D. Dimitropoulos, and B. Jalali, "Demonstration of CW Raman Gain with Zero Electrical Power Dissipation in p-i-n Silicon Waveguides," presented at the IEEE Conf. Lasers and Electro-Optics (CLEO), 2006, Paper #CMK3.

[33] S. Fathpour and B. Jalali, "Energy harvesting in silicon optical modulators," *Opt. Exp.*, vol. 14, pp. 10795–10799, Oct. 2006.

[34] J. Yu, "Recent progresses of silicon-based optoelectronic devices for application in fiber communication," in *Proc. IEEE Group IV Photon. Conf.*, 2004, pp. 139–141.

Sasan Fathpour (M'04) received the B.S. degree from Isfahan University of Technology, Isfahan, Iran, in 1995, the M.A.Sc. degree from the University of British Columbia (UBC), Vancouver, BC, Canada, in 2000, and the Ph.D. degree from the University of Michigan, Ann Arbor, in 2005, all in electrical engineering. His Ph.D. dissertation was on epitaxial growth, fabrication, characterization and modeling of In(Ga)As self-assembled quantum dot lasers, with record high dynamic and static performances, as well as on spin-polarized light sources based on diluted magnetic III-V semiconductors.

He joined the University of California, Los Angeles (UCLA), as a Postdoctoral Research Fellow in 2005. From 1995 to 1997, he was with Isfahan Optical Industry and was engaged in the research and development of microelectronic circuits and DSP systems in Pardisan Inc. in 1998. He is currently a Visiting Assistant Professor with UCLA, performing research on silicon photonics, particularly applications of nonlinear optical effects in active silicon optoelectronic devices. His research at UBC was on nitride heterojunction bipolar transistors. He is a coauthor of about 50 journal and conference publications.

Dr. Fathpour was the recipient of the 2007 UCLA Chancellor's Award for Postdoctoral Research.

Kevin Tsia (M'05) received the B.E. and M.Phil. degrees in electrical and electronic engineering from the Hong Kong University of Science and Technology, Hong Kong, in 2003 and 2005, respectively. He is currently working toward the Ph.D. degree at the Electrical Engineering Department, at University of California, Los Angeles.

His current research interests include active silicon photonic devices, particularly silicon Raman amplifiers and parametric wavelength converters with the two-photon photovoltaic effect.

Mr. Tsia was the recipient of a Fellowship by the California Nanosystems Institute (CNSI) from 2005 to 2006.

Bahram Jalali (S'86–M'89–SM'97–F'04) is a Professor of Electrical Engineering and the Director of the Optoelectronic Circuits and System Laboratory at the University of California, Los Angeles (UCLA). From 1988 to 1992, he was a Member of Technical Staff with the Physics Research Division, AT&T Bell Laboratories, Murray Hill, NJ, where he conducted research on ultrafast electronics and optoelectronics. His current research interests are in silicon photonics and ultrafast photonic signal processing. He has published over 200 scientific papers and holds six U.S. patents. While on leave from UCLA from 1999 to 2001, he founded Cognet Microsystems, a Los Angeles-based fiber-optic component company. He served as the company's CEO, Presidentm and Chairman from the company's inception through its acquisition by Intel Corporation in April 2001. From 2001 to 2004, he served as a consultant to Intel Corporation. He serves on the Board of Trustees of the California Science Center.

Dr. Jalali is a Fellow of the Optical Society of America and the Chair of the Los Angeles Chapter of the IEEE Lasers and Electro-Optics Society. In 2005, he was chosen by *Scientific American Magazine* as the 50 Leaders Shaping the Future of Technology. He is a member of the California Nano Systems Institute (CNSI). He was the recipient of the BridgeGate 20 Award for his contribution to the southern California economy.